Nanoscale

Accepted Manuscript

Journal Name

ARTICLE

Susceptibility losses in heating of magnetic core/shell nanoparticles for hyperthermia: A Monte Carlo study of Shape and Size effects

M. Vasilakaki,[a] C. Binns,[b] and K. N. Trohidou[a] ,

Optimizing the heating properties of magnetic nanoparticles is of great importance for hyperthermia applications. Recent experimental results show that core/shell nanoparticles could give an increased specific absorption rate (SAR) compared to the magnetic oxide nanoparticles currently used. We have developed a modified phenomenological model based on the linear Néel-Brown relaxation model to calculate the SAR due to susceptibility losses in complex nanoparticles with ferromagnetic (FM) core/ ferrimagnetic (FiM) shell morphology. We use the Monte Carlo (MC) simulations technique with the implementation of the Metropolis algorithm to investigate the effect of the size and shape on the magnetisation behaviour of complex ferromagnetic/ferrimagnetic nanoparticles covered by a surfactant layer. The findings of our simulations are used as an input in our modified model for the calculation of the SAR.

Our calculations show that for all the sizes and shapes the complex FM/FiM nanoparticles give higher SAR values than the pure ferrimagnetic ones due to their higher core saturation magnetisation. For all sizes the nanoparticles with the truncated cuboctahedral shape give the highest SAR values and the cubic ones the lowest ones. The decrease in the surfactant thickness results in an increase of the SAR values. Our results have the same characteristics as the available experimental data from Fe/Fe_3O_4 nanoparticles, confirming that the complex nanoparticles with core/shell morphology can optimise the heating properties for hyperthermia.

Introduction

Magnetic nanoparticles have been used in many important technological applications such as ultra-high density magnetic recording and data storage, highly sensitive magnetic sensors and permanent magnets. Recently, magnetic nanoparticles (MNPs) are attracting attention in both nanomedicine and biology for theranostic applications[1-5] including magnetic separation of biological entities, therapeutic drug delivery, magnetic hyperthermia for tumour therapy, contrast agents for magnetic resonance imaging (MRI)[6-8] and markers in magnetic particle imaging (MPI).[9-12]

In particular magnetic particle hyperthermia is a promising cancer treatment technique. It is based on the fact that by injecting magnetic nanoparticles in the tumour and subjecting them to an alternating (AC) magnetic field they release heat, generating temperatures up to 42°C that can kill cancer cells by apoptosis, usually with minimal injury to normal tissue. Thus the technique can shrink tumours with minima side effects.

Active research is carried out to improve the specific absorption rate (SAR) of MNPs, which could permit the treatment of small tumours and reduce the amount of material that must be injected to treat a tumour of a given size. It has been demonstrated that the SAR of an assembly of nanoparticles depends on the mean nanoparticle size and the width of the size distribution,[13,14] the shape, the crystalline anisotropy,[15] the surface coating thickness,[16,17] the concentration and the degree of agglomeration (due to interparticle interactions).[18,19,20] The most studied and commercially produced colloids for magnetic hyperthermia contain iron oxide nanoparticles, especially magnetite (Fe_3O_4) and maghemite (γ -Fe_2O_3) because of their biocompatibility and high magnetisation.[21-25] Notably magnetite nanoparticles produced by magnetotactic bacteria measured by Hergt et al.[26] show the higher SAR up to now[27] but still other more complex oxide materials are investigated.[15, 28-32]

In the majority of models published so far the magnetic heating in nanoparticles is ascribed to two main mechanisms, that is, hysteresis losses[33,34] and susceptibility losses[14,35] though at a fundamental level they have the same root cause. In the

case of a ferromagnetic or ferrimagnetic material, when an alternating (AC) magnetic field is applied the non-linearity of the magnetisation M with respect to the applied field H, creates a hysteresis loop. The area within the $M(H)$ cycle determines the heat dissipation per AC magnetic field cycle and the SAR due to hysteresis losses is proportional to the frequency (f) multiplied by the area of the loop.[36] In the case of superparamagnetic nanoparticles or for sufficiently small field amplitudes, the magnetisation is assumed to be linear with H, taking into account irreversibility by assuming a complex magnetic susceptibility, and the SAR due to susceptibility losses is calculated according to the Linear Response Theory for the Néel-Brown relaxation model.[37] The contribution of each mechanism depends on the amplitude of the AC magnetic field, the size and magnetic anisotropy of the particle.[14]

In recent years the idea of using complex nanoparticles with a high core saturation magnetisation that gives a greater heating effect than pure oxides nanoparticles[38,39] and an oxide coating that renders them biocompatible, allowing them to be observed using MRI has been tested and is gaining acceptance.[40,41] It has been demonstrated experimentally that complex nanoparticles with a soft Fe core /hard Fe_3O_4 shell morphology[27,42] or hard $CoFe_2O_4$ core/soft $MnFe_2O_4$ shell[43] morphology give higher SAR values than the single-phase oxides. Also it has been demonstrated that the shape of the nanoparticles plays an important role in the SAR amplitude[44] as in the case of simple nanoparticles.[45-47]

In this paper we investigate theoretically for the first time the mechanism of magnetic heating due to susceptibility losses in complex ferromagnetic (FM) core/ ferrimagnetic (FiM) shell nanoparticles of different sizes between 11-29 nm covered by an organic surfactant including in our simulation explicitly the FM core, the FM /FiM interface and the FiM shell contributions. We use the Monte Carlo (MC) simulations technique with the Metropolis algorithm to simulate the magnetisation behaviour of complex FM/FiM nanoparticles of different shapes. We calculate the magnetisation and we use our results in a modified linear Néel-Brown relaxation model to calculate the susceptibility loss of complex soft Fe/ hard Fe_3O_4 nanoparticles under the application of a small AC magnetic field with an amplitude H_0 that gives a Zeeman energy smaller than the anisotropy energy barrier.[37,48] The values of the applied field are in the range of small amplitudes that satisfy the 'Atkinson-Brezovich criterion' that is H_0 x f = 4.85 x 10^8 Am^{-1}s^{-1}, which is safe for application in humans.[34] Our results are compared with the results for FiM nanoparticles that are usually used in magnetic particle hyperthermia.

The SAR Model and Monte Carlo Simulations

We have modelled four different shapes of complex nanoparticles that consist of a FM core and a FiM shell: sphere, cube, octahedron and truncated cuboctahedron as they are shown in Fig. 1 of size D on a simple cubic lattice.

We consider four regions for each nanoparticle: the core (black), the core interface (red), the shell interface (green) and the shell (blue) (Fig. 2).
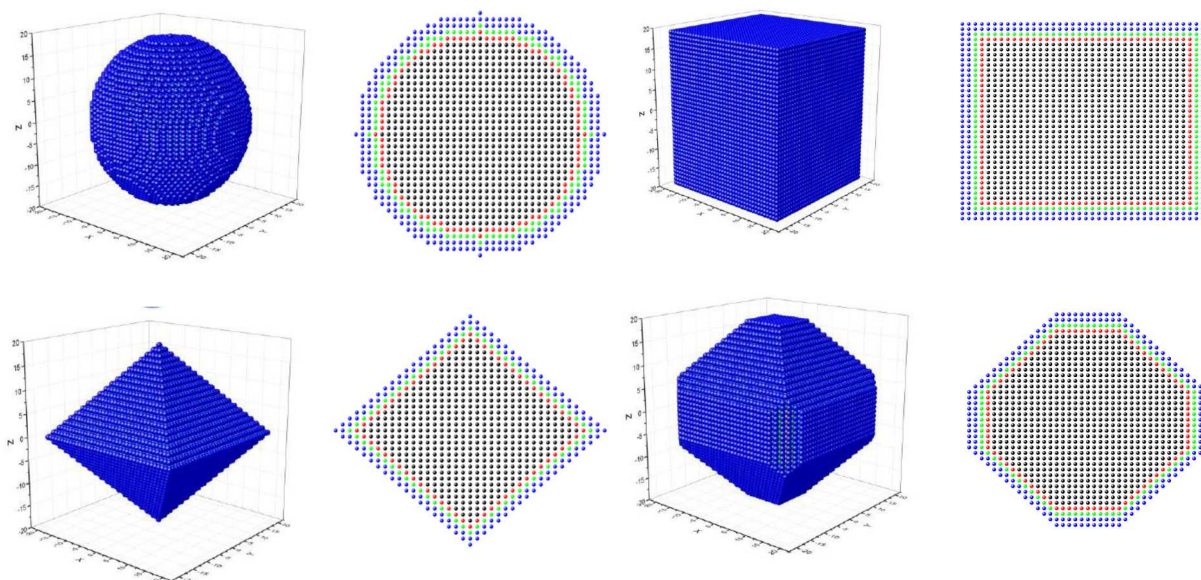
Fig. 1 Modelled 3D (blue) and 2D (in the x=0 plane) (core (black), core interface (red), shell interface (green), shell (blue)) shapes of spherical, cubic, octahedral, truncated cuboctahedral complex FM/FiM nanoparticles.
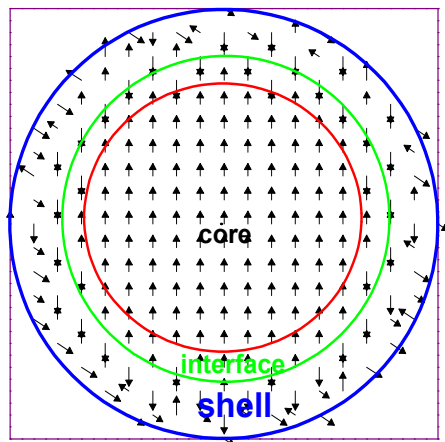
Fig. 2 2D (in the x=0 plane) schematic representation of the different regions (core (black), core interface (red), shell interface (green), shell(blue) in a complex spherical nanoparticle with a FMcore and a FiM shell.

We notice here that though in our results we refer to the shell thickness of 2.5 nm, in this thickness we have included the surface contribution, which is taken into account explicitly by including surface anisotropy with size and type different from that of the shell. We assume that the interface and the surface thickness are equal to one lattice spacing, by considering the lattice parameters for Fe and Fe_3O_4 ($a_{Fe} = 0.287 \times 10^{-9}$ m, $a_{Fe3O4} = 0.8397 \times 10^{-9}$ m), the shell thickness, including the shell interface and shell of 1.67 nm and the surface 0.83 nm, is 2.5 nm.

We have used atomic-scale modelling, where the spins interact with nearest-neighbours via Heisenberg interactions and at each crystal site they experience a uniaxial anisotropy. The energy of the system includes the exchange interaction between the spins in the core, the shell and at the interface, the single-site anisotropy energy terms of the core, the shell, the FM and the FiM interfaces and the surface, and the Zeeman energy term.

$$E= - J_{core} \sum_{i,j \in core} \vec{S}_i \cdot \vec{S}_j - J_{shell} \sum_{i,j \in shell} \vec{S}_i \cdot \vec{S}_j - J_{IF} \sum_{i \in core, j \in shell} \vec{S}_i \cdot \vec{S}_j$$
$$- \sum_{i \in core} K_{core} \left(\vec{S}_i \cdot \hat{e}_i \right)^2 - \sum_{i \in shell} K_{shell} \left(\vec{S}_i \cdot \hat{e}_i \right)^2 - \sum_{i \in IF} K_{IF} \left(\vec{S}_i \cdot \hat{e}_i \right)^2$$
$$- \sum_{i \in surface} K_{srf} \left(\vec{S}_i \cdot \hat{e}_i \right)^2 - \vec{H} \cdot \sum_i \vec{S}_i$$

$$(1)$$

Here $\vec{S}_i$ is the atomic spin at site i and $\hat{e}_i$ is the unit vector in the direction of the easy axis at site i. We considered the magnitude of the atomic spins in the FiM sublattices to be equal to 1 and 1.5 respectively.[49] The core and the shell anisotropy were assumed to be uniaxial along the z axis and the surface anisotropy randomly oriented according to experimental

indications for nanoparticles produced with the ion-beam technique.[27] The exchange coupling constant of the core is $J_{core}=J_{FM}$ where J_{FM} is considered to be the exchange coupling constant of a pure ferromagnet and is taken equal to 1 and of the shell is $J_{shell}=-J_{FM}/2$ due to the fact that the Curie temperature of the FM (T_C Fe = 1043 K) in the core is higher than the critical temperature of the FiM in the shell (T_C Fe_3O_4 = 858 K). We set the interface coupling constant $J_{IF}=J_{FM}/2$, so the interfacial interaction is taken to be ferromagnetic. We note here that the estimation of J_{shell} and J_{IF} is made using the mean field theory arguments and taking into account the size effects of the bulk values. The anisotropy constants K are given in units of J_{FM}. The anisotropy constant of the core is $K_{core}=0.05J_{FM}$, of the core and shell interface $K_{IF}=0.5$ J_{FM} and of the shell $K_{shell}=0.5$ J_{FM} respectively, that is one order of magnitude larger than the K_{core}. The surface anisotropy is $K_{srf}=1.5J_{FM}$ due to the lower crystal symmetry at the surface.[49] We have used the Metropolis Monte Carlo simulation technique to simulate the hysteresis loops at different temperatures. We have calculated the normalized saturation magnetisation of the core M_{core}, interface M_{IF}, shell M_{shell} or surface M_{srf}. The temperature T is given in units J_{FM}/k_B. We have used 10^4 MC steps per spin (MCSS) at each field step and the results were averaged over 50 different samples (namely random numbers).

We have also simulated the magnetic behaviour of ferrimagnetic nanoparticles with a disordered surface. In this case in eq. 1 we have one exchange interaction term, two anisotropy terms for the core and the surface of the FiM nanoparticles and the Zeeman term. We considered the exchange coupling constant equal to $J_{FiM}= -0.5$ J_{FM} and the core anisotropy along the z-axis with anisotropy constant $K_{core} =0.02$ J_{FM}. The surface anisotropy is taken to be random with $K_{srf}=0.2$ J_{FM}.

We have calculated the SAR due to susceptibility losses of FM/FiM and FiM nanoparticles starting from the linear Néel-Brown relaxation model[35] which is based on two heating mechanisms: 1) the Brownian relaxation mechanism and 2) the Néel relaxation mechanism. In our modified model we have taken into account explicitly the different regions of the complex FMcore/FiMshell and the FiM core/surface nanoparticles. For these two relaxation mechanisms we introduced effective magnetisation and anisotropy terms into the expressions for the relaxation times to describe the motion of the nanoparticle magnetisation component, taking into account the nanoparticle's morphology.

The Brownian relaxation time is
$$\tau_B = \frac{3\eta}{k_B T} V_{TOT}$$

The total volume V_{TOT} of the nanoparticle surrounded by the surfactant layer is given by

$$V_{TOT} = V_{core} + V_{shell} + V_{IF} + V_{surfac}$$

So for the FM/FiM nanoparticles τ_B becomes:

Nanoscale Accepted Manuscript

$$\tau_B = \frac{3\eta}{k_B T}\left(V_{core} + V_{shell} + V_{IF} + V_{surfac}\right) \quad (2)$$

where η is the medium viscosity with a value of 0.65×10^{-3} Pa.s (approximately the value for water in 40^0C) and V_{core}, V_{shell}, V_{IF}, are the volumes of the different particle's regions and V_{surfac} the surfactant volume.

The Néel relaxation time is given by

$$\tau_N = \frac{\sqrt{\pi}\tau_0 e^\Gamma}{2\sqrt{\Gamma}} \quad \text{where } \Gamma = \frac{K\ V}{k_B T}$$

where V is the nanoparticle volume, without the surfactant, τ_0 is the natural time constant of the magnetic moment equals to 10^{-9}s and taking into account the fact that the effective volume anisotropy for the FM/FiM nanoparticles given from ref 50 is

$$\left(K\ V\right)_{eff} = K_{core}V_{core} + K_{shell}V_{shell} + K_{IF}V_{IF}$$

then the Néel relaxation time becomes :

$$\tau_N = \frac{\sqrt{\pi}\tau_0 e^\Gamma}{2\sqrt{\Gamma}} \quad (3)$$

Where $$\Gamma = \frac{K_{core}V_{core} + K_{shell}V_{shell} + K_{IF}V_{IF}}{k_B T}$$

The SAR is expressed as

$$SAR(f) = \frac{\mu_0 \pi f \chi'' H_0^2}{\rho} \quad (4)$$

Here ρ is the average density of the NP, $\mu_0 = 4\pi \times 10^{-7}$ H/m f is the frequency and χ'' is the imaginary part of the complex susceptibility which is given by

$$\chi'' = \frac{\omega\tau}{1 + \left(\omega\tau\right)^2}\chi_0 \quad (5)$$

where $\omega = 2\pi f$ and τ is the relaxation time which is defined as :

$$\frac{1}{\tau} = \frac{1}{\tau_B} + \frac{1}{\tau_N} \quad and \quad \tau = \frac{\tau_B \tau_N}{\tau_B + \tau_N} \quad (6)$$

where τ_B and τ_N are given by Eqs (2) and (3) respectively and χ_0 is the dc initial magnetic susceptibility given by a Langevin function of the formula:

$$\chi_0 = \frac{3\chi_i}{\xi}\left(\coth\xi - \frac{1}{\xi}\right)$$

$$\chi_i = \frac{\mu_0 \varphi M_S^2 V}{3k_B T} \quad \text{and} \quad \xi = \frac{\mu_0 M_S VH}{k_B T}$$

Here M_s the nanoparticle saturation magnetisation and φ is the mean ratio of the NPs in the solution and equals to 0.001 in our case. Taking into account that[50]

$$(MV)_{eff} = M_{core}V_{core} + M_{shell}V_{shell} + M_{IF}V_{IF}$$

for the FM/FiM nanoparticles, the dc initial magnetic susceptibility becomes:

$$\chi_0 = \frac{\varphi\left(M_{core}V_{core} + M_{shell}V_{shell} + M_{IF}V_{IF}\right)}{(V_{core} + V_{shell} + V_{IF})H_0}\left(\coth\xi - \frac{1}{\xi}\right) \quad (7)$$

$$\text{and} \quad \xi = \frac{\mu_0 H_0\left(M_{core}V_{core} + M_{shell}V_{shell} + M_{IF}V_{IF}\right)}{k_B T}$$

We set the anisotropy constant of the ferromagnetic core of the complex nanoparticles equal to the bulk anisotropy of Fe $K_{core} = K_{Fe} = 4.9 \times 10^4$ J/m^3 and for the ferrimagnetic core $K_{core} = K_{Fe3O4} = 1.87 \times 10^4$ J/m^3.[51] The anisotropy constants of the interface K_{IF}, shell K_{shell} and surface K_{srf} are calculated using the same ratios of the anisotropy constants used in the MC simulations. So for the FM/FiM nanoparticle the anisotropy constants used to calculate SAR are set to be $K_i = 10 \times K_{Fe}$ where i=IF, shell, and $K_{srf} = 30 \times K_{Fe}$ and for the FiM nanoparticle $K_i = K_{Fe3O4}$ where i=core, IF, shell and $K_{srf} = 10 \times K_{Fe3O4}$. The average particle density is calculated considering the average of $\rho_{Fe} = 7.87 \times 10^3$ kg/m^3 and $\rho_{Fe3O4} = 5.24 \times 10^3$ kg/m^3. Temperature is set to T = 313 K.

The saturation magnetisations of the core M_{core}, the interface M_{IF} and the shell M_{shell} are set equal to the product of the MC calculated values of the normalized corresponding magnetisations $M_{i(MC)} \times$ the bulk saturation magnetisation of the FM core $M_{S\ Fe} = 1.77 \times 10^6$ A/m and the FiM shell $M_{S\ Fe3O4} = 4.11 \times 10^5$ A/m respectively. So $M_i = M_{i\ (MC)} \times M_S$ where i=core,IF,shell. We have calculated the saturation magnetisations in this way in order to include in our model the effect of the nanoparticles size and the different regions of the saturation magnetisation. We use as a reference the bulk saturation magnetisation of the materials taking into account the fact that for the smaller complex particle the ideal stoichiometry of 25% between saturation magnetisation of Fe and FeO exists according to the Ref. 27.

In the case of the FiM nanoparticles in all calculations we take into account the fact that $(KV)_{eff} = K_{core}V_{core} + K_{srf}V_{srf}$ and $(MV)_{eff} = M_{core}V_{core} + M_{srf}V_{srf}$, consequently Equations (2-7) are modified accordingly.

The calculation of the SAR due to susceptibility losses of an assembly of non-interacting complex and FiM nanoparticles with a log-normal size distribution w(D) with the parameters of mean $\mu = 2.675$ and standard deviation $\sigma = 0.2$ of the experimental system[52] has been made with the formula below

$$SAR(f) = \sum_D w(D) \, SAR \, (D,f) \qquad (8)$$

where SAR(D,f) is the SAR of the corresponding size D of each nanoparticle.

Results and discussion

We performed calculations of the SAR using the characteristics for Fe/Fe_3O_4 nanoparticles with sizes in the range of 11-29 nm and shell thickness of 2.5 nm in all cases, as in the experimental situation of ref 27. We applied a small AC magnetic field with amplitude H_0 in the range of 24 Oe-125 Oe, that according to the Atkinson-Brezovich criterion corresponds to the frequency range 50kHz-250kHz. The field must be almost six times smaller than the estimated coercive field ($H_C \approx 600$ Oe at T= 300K for 10 nm Fe/Fe_3O_4 nanoparticles[53]). In this case Néel and Brown relaxation dominates in the heat generation process.[37] In order to calculate theoretically the SAR of the core/shell nanoparticles we have developed a modified Néel-Brown relaxation model where we take into account explicitly the complex morphology of the nanoparticles (see previous Section). In this model we include explicitly the volume (see Fig. S1 in the Supplementary Materials File) and the saturation magnetisation for each layer (see Fig. S2, S3). The magnetisation is calculated with the Metropolis Monte Carlo simulation technique including the corresponding anisotropy constants at the temperature 313 K. At this temperature, which is around one third of the Curie temperature for Fe ($T_C \sim 1043$ K), the hyperthermia experiments are performed. In our simulations the critical temperature of the complex FM/FiM nanoparticles, for the range of sizes from 11 to 29 nm, is 2.0 J_{FM}/k_B. Thus we performed our simulations at the temperature T=0.75 J_{FM}/k_B.

The SAR as a function of the AC field frequency is calculated using Eq. (4). In the SAR calculations according to the 'Atkinson-Brezovich criterion[34] for all frequencies the product H_0 x f has the value 4.85 x 10^8 Am^{-1}s^{-1}. As an example, we mention that at the frequency of 100 kHz the field amplitude should be 4850 Am^{-1}.

In Figs. 3(a-d) we have plotted the SAR as a function of the AC magnetic field frequency for complex spherical, cubic, octahedral and truncated cuboctahedral nanoparticles respectively, with various particle sizes in the range of 11-29 nm, considering a surfactant thickness of t_{surfac}=4 nm. In these figures we show our results for the frequency range between 50-200 kHz, which is the range of interest for applications in humans. We can see that the magnitude of the SAR values depends on the shape and size of the nanoparticles. It appears that the truncated cuboctahedral nanoparticles have the highest SAR values and the cubic particles have the lowest ones, for all nanoparticle sizes. We attribute the low SAR values for the cubic nanoparticles to their volume and magnetisation sizes (see Figs. S1, S2). The cubic nanoparticles have the biggest volume (Fig. S1) for a given size, as a result they have the

highest Brownian relaxation time (Eq. 2). The Néel relaxation time is also larger than that in the other shapes since the cubic nanoparticles have the largest (KV)$_{eff}$ products (see Fig. S4) for all nanoparticle sizes. Consequently, the inverse relaxation time is the smallest in the case of cubic nanoparticles (Eq. 6). Also they have the biggest (MV)$_{eff}$ values (Fig. S4). From Eq. 7 we deduce that they give lower SAR values than the other shapes for all the sizes. Also from Figs. 3, we observe that there is no systematic size dependence of the SAR values of the nanoparticles, for all the shapes. This is due to the different contributions of the different regions to the volume and to the magnetisation as the nanoparticle size increases, for the different regions namely the core, IF and shell (see Figs S1 and S2).

In the supplement in Fig. S5 we show our results for the lower frequency range (0-49 kHz), of the SAR. In this frequency range a peak appears in the SAR versus frequency curve. As can be seen from Fig. S5 the position and size of the peak of the SAR curve depends on the size and shape of the nanoparticles. As the particle becomes smaller the peak of the SAR becomes lower and moves to higher frequencies and the SAR versus frequency curve is broader around its maximum value.

However, we should point out that in the frequency range 0 - 30 kHz where high fields with amplitude larger than 300 Oe are applied, we are outside the area where the Linear Response Theory is valid, so we expect that our calculations underestimate the value of the SAR in this frequency region.[37,54]

We note here that the SAR calculations have been carried out considering constant viscosity of the medium and it corresponds to that of water at around 40°C. Larger values of viscosity, that we tried, lead to a suppression of the SAR values so it is important to know the medium viscosity in experiments as it is reported by G Vallejo-Fernandez et al.[33]

We have also studied the SAR behaviour for Fe_3O_4 nanoparticles that are usually used in biomedical ferrofluids,[55] for the same range of particle sizes and the same shapes. These nanoparticles have lower saturation magnetisation (see Figs. S3) and lower anisotropy constants than the core/shell nanoparticles.[51,53] In our simulations for the FiM nanoparticles we take into account surface effects by considering surface random anisotropy of an order of magnitude larger than the uniaxial core anisotropy. We can see that the total ferrimagnetic saturation magnetisation decreases with the increase in size of the nanoparticle (see Fig. S3). In FiM nanoparticles[56] the increase of the magnetisation in the smaller particles, is attributed to the uncompensated spins at the surface[57] as in the case of antiferromagnetic nanoparticles.[58] Thus as the nanoparticle size increases the contribution of the surface decreases, consequently the magnetic component also decreases. In addition, the cubic ferrimagnetic nanoparticles have the smallest total saturation magnetisation. This is consistent with our previous studies[57,59] where it was demonstrated that cubic FiM nanoparticles have lower

magnetisation than the spherical ones due to the lower number of uncompensated spins.

In Figs. 4(a-d) we show the dependence of the SAR on the AC magnetic field frequency for FiM nanoparticles with different sizes and the four shapes, as in the case of the complex nanoparticles. These nanoparticles have a surface thickness 0.83 nm and surfactant layer thickness 4 nm.
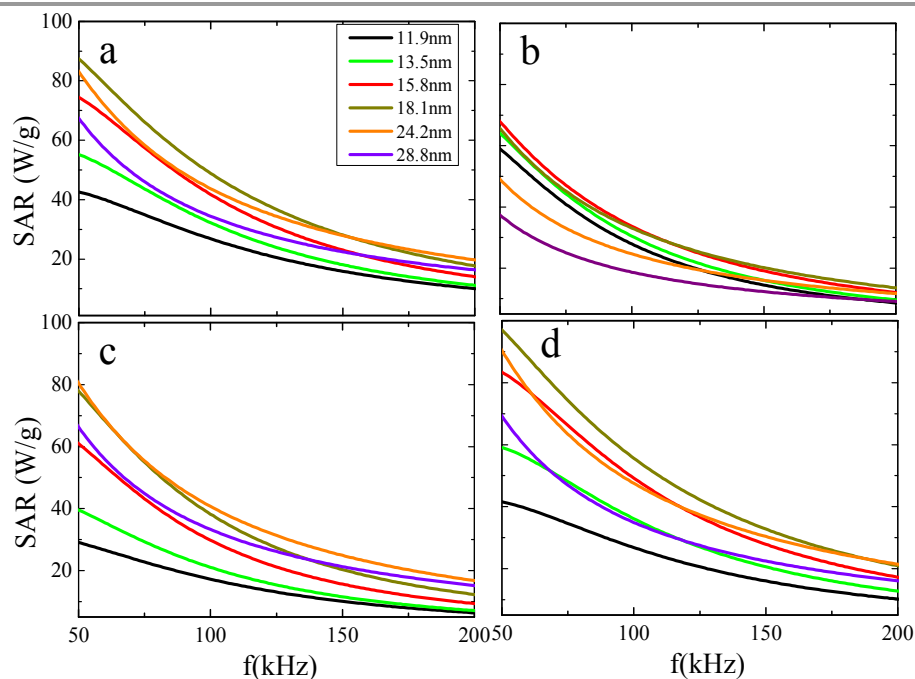
Fig. 3 SAR due to susceptibility losses of FM/FiM nanoparticles as a function of the AC magnetic field frequency for different sizes of (a) spherical, (b) cubic, (c) octahedral, (d) truncated cuboctahedral nanoparticles with FiM shell thickness 2.5 nm and surfactant layer thickness 4nm. The applied AC magnetic field follows the $H_0 \times f = 4.85 \times 10^8$ Am^{-1}s^{-1} criterion (safe for application in humans).
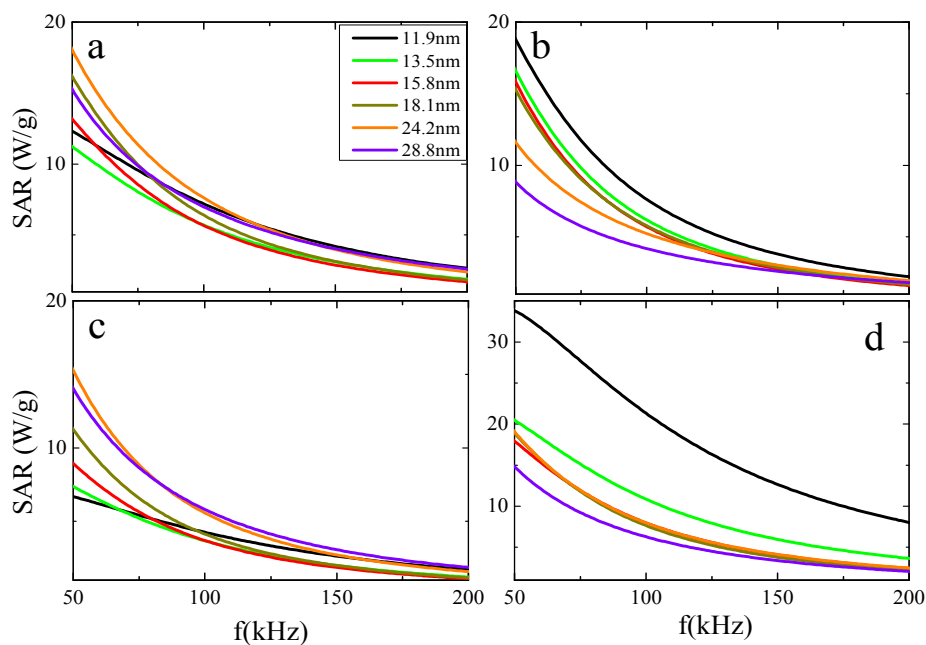
Fig. 4 SAR due to susceptibility losses of the FiM nanoparticles as a function of the AC magnetic field frequency for different sizes for (a) spherical, (b) cubic, (c) octahedral, (d) truncated cuboctahedral shapes with FiM surface thickness 0.83 nm and surfactant thickness 4nm. The applied AC magnetic field follows the $H_0 \times f = 4.85 \times 10^8$ Am^{-1}s^{-1} criterion (safe for application in humans).

In the case of ferrimagnetic nanoparticles our simulations show that their lower saturation magnetisation (Fig. S3, S4) results in a decrease of the dc initial magnetic susceptibility (Eq. 7) so the SAR values are almost three times lower than those of the complex ones of the same shape.

Also we see that, for a range of small sizes (12-16 nm), the combination of the small particle volume and the increased saturation magnetisation with decreasing particle size that enters into Eq. 7 causes a different SAR size dependence from that of complex nanoparticles. In the case of octahedral small FiM nanoparticles, their lower volume compared to the other shapes and the lower $(KV)_{eff}$ and $(MV)_{eff}$ values (see Fig. S1, S4) result in smaller values of χ_0 (Eq. 7) and comparable Néel and Brownian relaxation times (Eq. 2, 3), leading to a decrease in the SAR values as the size decreases. For all the shapes, the spherical, the cubic and truncated cuboctahedral small nanoparticles, because of their higher values of magnetisation in comparison to larger ones of the same shape (see Fig. S3), give larger dc initial magnetic susceptibility χ_0 and larger SAR as the particle size decreases.

In Fig. 5 we have plotted the SAR as a function of the nanoparticle size for the four different shapes of FM/FiM (solid lines) and FiM (dotted lines) nanoparticles for two different frequencies. These are the frequencies usually used in hyperthermia applications (f=50 and 100 kHz) to stress the difference of the SAR size and shape dependence between complex FM/FiM and FiM nanoparticles.

From Fig. 5 it is apparent that the complex nanoparticles can optimize the SAR for all shapes and sizes for these two frequencies. Also we can see that for the core/shell nanoparticles, the SAR peaks at a specific size. As we can see in Figure S4, this behaviour is due to the fact that for sizes above around 15 nm the $(KV)_{eff}$ increases rapidly but the increase of $(MV)_{eff}$ is slower as a result the SAR decreases slowly (see Eqs. 4 and 7) with increasing size. This is the case for the nanoparticles with spherical, octahedral and truncated cuboctahedral shape. For the cubic nanoparticles the fast increase of both quantities above 15 nm (Fig. S4) causes a fast decrease of SAR with increasing size.

We also investigated the effect of the surfactant layer thickness on the SAR. We show in Fig. 6 the dependence of SAR on the AC magnetic field frequency for FM/FiM covered with a surfactant layer of thickness $t_{surfac} = 10$ and 14 nm. The results in these figures are given for various nanoparticle sizes for the four shapes. We note here that the thickness 14 nm is the one reported in recent experiments on 16.5 nm Fe/FeO nanoparticles.[27]

We observe here that the magnitude of the SAR value increases as the surfactant thickness decreases. Also we observe that for small surfactant thickness the role of the nanoparticle's size becomes significant for all the shapes.
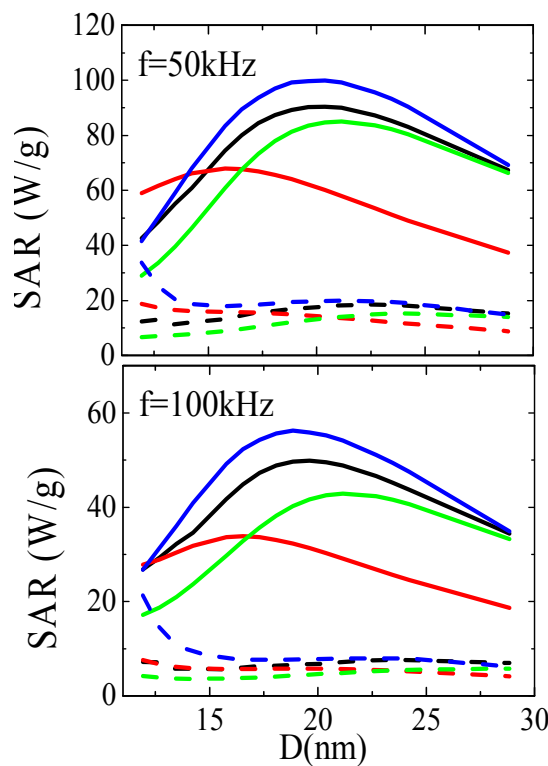
Fig. 5 SAR due to susceptibility losses as a function of the size for the FM/FiM nanoparticles (solid lines) with spherical (black), cubic (red), octahedral (green), truncated cuboctahedral (blue) shapes and for the FiM nanoparticles (dotted lines) for two AC magnetic field frequency values (H_0 x f = 4.85 x 10^8 Am^{-1}s^{-1}) and surfactant thickness 4.0 nm.

These differences are attributed to the fact that the reduction of the surfactant layer causes a reduction of the Brownian relaxation time (Eq. 1) so the total inverse relaxation time (Eq. 3) increases causing the increase of the SAR values with frequency. As can be seen in the figure 5 this decrease of the relaxation time causes a stronger dependence of the SAR on particle sizes.

In the Supplement in Fig. S6 we give the SAR dependence on the AC magnetic field frequency for FiM nanoparticles covered with a surfactant layer of thickness $t_{surfac} = 10$ and 14 nm.

The variation of the surfactant layer thickness has the same effects on the SAR behaviour in the case of FiM nanoparticles. In Fig. S6 we can see that the SAR values for the FiM nanoparticles increase with the decrease of the surfactant layer thickness.

By increasing the surfactant layer thickness we have decrease of the magnitude of the SAR value and the nanoparticle size dependence is not significant for the complex and the FiM nanoparticles.
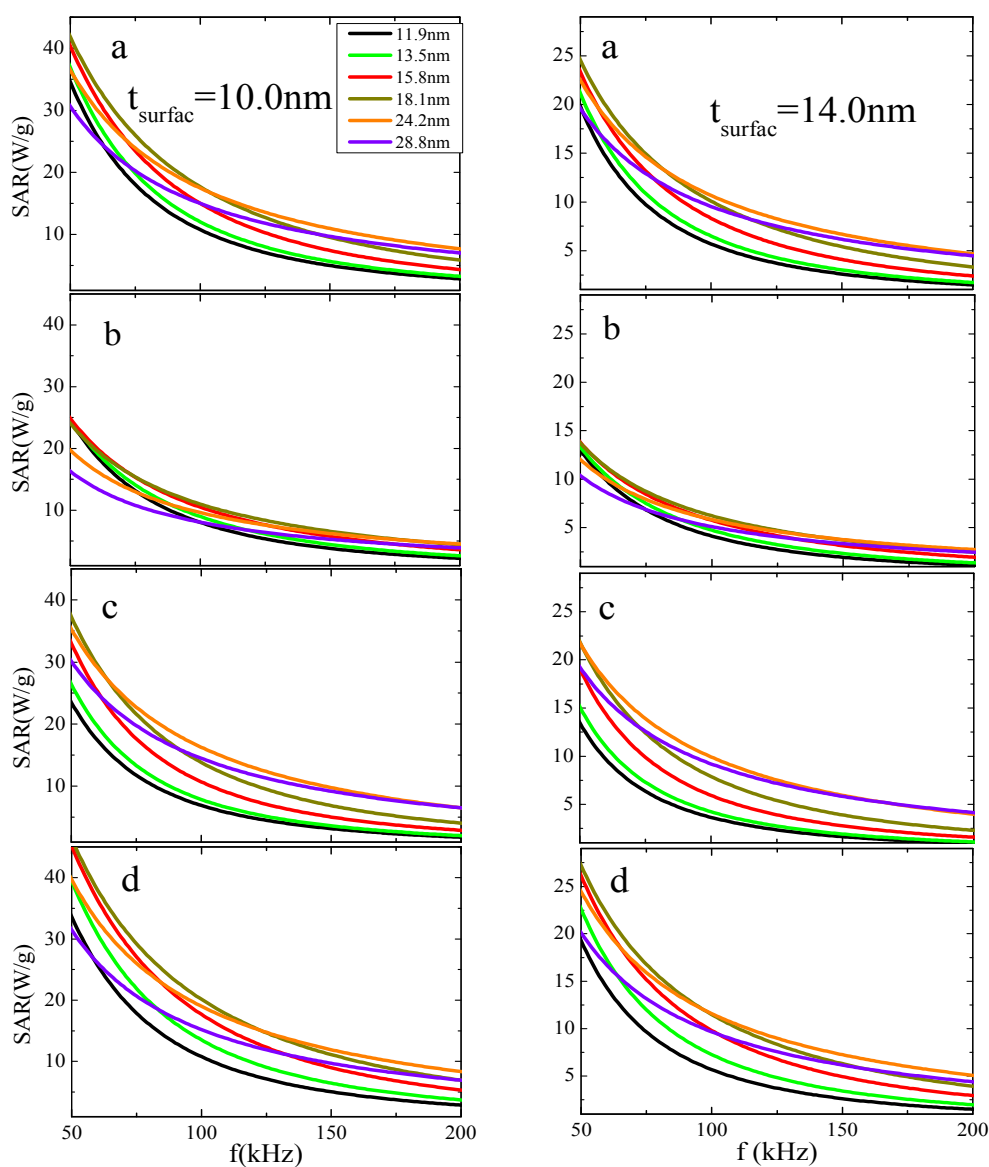
Fig. 6 SAR of spherical (a) cubic (b) octahedral (c) and truncated cuboctahedral (d) FM/FiM nanoparticle respectively with surfactant thickness t_{surfac}= 10 nm (left side figures), and t_{surfac}=14 nm (right side figures)due to susceptibility losses as a function of the AC magnetic field frequency for different sizes . The applied AC magnetic field follows H_0 x f = 4.85 x 10^8 $Am^{-1}s^{-1}$ (safe for application in humans).

Finally we have calculated the average SAR value of an assembly of non-interacting FM / FiM (Fig. 7 (a, b)) nanoparticles with a rather broad log-normal size distribution (solid lines) for a mean nanoparticle size of 16.5 nm as found in recent experiments.[27] We compare the results with those of a uniform nanoparticle with size 16.5 nm (dotted lines). In both cases we have considered a surfactant thickness of 4 and 14 nm respectively. It has been demonstrated theoretically in Ref. 35 and experimentally in Ref. 60 where the power dissipation of

magnetic fluids of Fe oxides, subjected to AC field is studied, that the particle size distribution modifies the thermal dissipation rate. In Fig. 7 we observe that for the surfactant thickness t_{surfac}=4nm the existence of the particle size distribution decreases the SAR values for the mean size 16.5 nm nanoparticles in the frequency range 50-200 kHz. This is due to the lower SAR contributions of larger nanoparticles as observed in Fig. 5. However, as the surfactant thickness increases we observe that the size distribution doesn't

contribute any more to the SAR. We expect that the existence of an additional distribution of surfactant thickness in a system with a size distribution of the nanoparticles will modify the hyperthermia properties.

The comparison of the calculated SAR values due to susceptibility losses for FM/FiM (Fig. 7) and FiM (not shown here) nanoparticles with a log-normal distribution and surfactant thickness 14 nm indicates that by choosing the optimum values of the frequency and the surfactant thickness the Fe/FeO nanoparticles give larger SAR values (~ 4 times)

than the Fe oxides (hematite, magnetite) nanoparticles in agreement with the experimental results of Ref 27 for f=100 kHz and $H_0 = 4.85 \times 10^6$ Am^{-1}. However the values of SAR due to susceptibility losses from our calculations for the complex nanoparticles are smaller than the experimental SAR values of Ref. 27. This difference is attributed to the difference in the number of neighbours, in the distribution of surfactant thickness and in the hysteresis losses of the larger complex nanoparticles in the experiment.
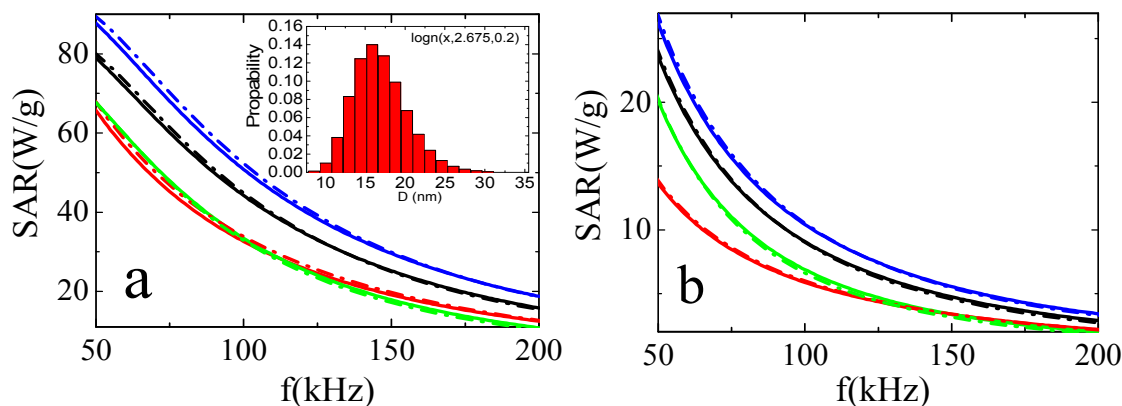
Fig. 7 SAR of FM/FiM in the case of a log-normal size distribution (see Inset) (solid lines) and of a uniform particle size (dotted lines) with surfactant layer thickness of t_{surfac}= 4 (a) and t_{surfac}=14 nm (b) as a function of the AC magnetic field frequency for spherical (black), cubic (red), octahedral (green), truncated cuboctahedral (blue) shape ($H_0 \times f$ = 4.85 x 10^8 Am^{-1}s^{-1}).

Conclusions

We have developed a modified phenomenological model based on the linear Néel-Brown relaxation model to calculate the SAR due to susceptibility losses in complex magnetic core/shell nanoparticles in a range of small applied field amplitudes that satisfy the 'Atkinson-Brezovich criterion'. By using the Metropolis Monte Carlo simulations technique we studied the magnetisation dependence of SAR of the complex ferromagnetic / ferrimagnetic nanoparticles for various sizes and shapes. We have compared our results with those of ferrimagnetic nanoparticles that are currently used for magnetic hyperthermia treatment. Our calculations show that in all cases the complex nanoparticles give higher SAR values than the ferrimagnetic ones due to their higher core saturation magnetisation, in agreement with experimental measurements using Fe/Fe$_3$O$_4$ nanoparticles and Fe$_2$O$_3$ nanoparticles. Our calculations also show that a) a decrease in the surfactant thickness produces an increase in the SAR values and b) at the frequency of 100 kHz usually used for hyperthermia, the optimum value of SAR is obtained for the truncated cuboctahedral complex nanoparticles with a surfactant layer of thickness 4 nm.

Acknowledgements

Notes and references

[a] Institute of Nanoscience & Nanotechnology, NCSR "Demokritos", Aghia Paraskevi, 15310 Athens, Greece.
[b] Department of Physics and Astronomy, University of Leicester, Leicester LE1 7RH, United Kingdom.

1   S. Dutz and R. Hergt, *Nanotechnology*, 2014, **25**, 452001(28pp).

2   M. K. Yu, J. Park and S. Jon, *Theranostics*, 2012, **2**, 3-44.

3   K. Chatterjee, S. Sarkar, K. Jagajjanani Rao and S. Paria, Advances in Colloid and Interface Science, 2014, **209**, 8-39.

4   A. Hervault and N. T. K. Thanh, *Nanoscale,* 2014,**6**, 11553.

5   H. Mamiya, *Journal of Nanomaterials,* 2013, **2013,** 752973 (17pp).

6   P. Kucheryavy, J. He, V. T. John, P. Maharjan, L. Spinu, G. Z. Goloverda, and V. L. Kolesnichenko, *Langmuir*, 2013, **29**, 710-716.

7   P. Arosio, G. Baldi, F. Chiellini, M. Corti, A. Dessy, P. Galinetto, M. Gazzarri, M. S. Grandi, C. Innocenti, A. Lascialfari, G. Lorenzi, F.Orsini, A.M. Piras, C. Ravagli and C. Sangregorio, *Dalton Trans.,* 2013, **42**, 10282-10291.

8   M. Corti, A. Lascialfari, E. Micotti, A. Castellano, M. Donativi, A. Quarta, P.D. Cozzoli, L. Manna, T. Pellegrino, C. Sangregorio, *J. Magn. Magn. Matter.*, 2008, **320**, e320-323.

9   Q.A. Pankhurst, J. Connolly, S.K. Jones, J. Dobson, *J. Phys. D: Appl. Phys.*, 2003, **36**, R167-R181.

10 D. Ortega and Q. A. Pankhurst, *Magnetic hyperthermia, in Nanoscience: Volume 1: Nanostructures through Chemistry*, P. O'Brien, Royal Society of Chemistry: Cambridge. p. 60-88, 2013.

11 T. M. Buzug, G. Bringout, M. Erbe, K. Gräfe, M. Graeser, M. Grüttner, A.Halkola, T. F. Sattel, W. Tenner, H. Wojtczyk, J. Haegele, F. M. Vogt, J. Barkhausen, K. Lüdtke-Buzug, *Z. Med. Phys.*, 2012, **22**, 323-334.

12 L. H. Reddy,J. L. Arias, J. Nicolas, and P. Couvreur, *Chem. Rev.*, 2012, **112** (11), 5818–5878.

13 B. Mehdaoui , A. Meffre , J. Carrey , S. Lachaize , L. Lacroix , M. Gougeon , B. Chaudret , and M. Respaud , *Adv. Funct. Mater.*, 2011, **21**, 4573–4581.

14 R. Hergt, S. Dutz and M. Röder, *J. Phys.:Comdens. Matter.*, 2008, **20**, 385214 (12pp).

15 E. L. Verde, G. T. Landi, M. S. Carriao, A. L. Drummond, J. A. Gomes,E. D. Vieira, M. H. Sousa and A. F. Bakuzis, *AIP Advances*, 2012, **2**, 032120 (23pp).

16 X. L. Liu, H. M. Fan, J. B. Yi, Y. Yang, E. S. G. Choo, J. M. Xue, D. D. Fan and J. Ding, *J. Mater. Chem.,* 2012, **22**, 8235-8244

17 J. Majeed, L. Pradhan, R. S. Ningthoujam, R. K. Vatsa, D. Bahadur and A. K. Tyagi, *Colloidsand Surfaces B: Biointerfaces,* 2014, **122**, 396-403.

18 E. Lima Jr, E. De Biasi, M. Vasquez Mansilla, M. E Saleta, M. Granada, H. E. Troiani, F. B. Effenberger, L. M. Rossi, H. R. Rechenberg and R. D. Zysler, *J. Phys. D:Appl. Phys.,* 2013, **46**, 045002 (13pp).

19 A. E. Deatsch and B. A. Evans, *J. Magn. Magn. Mater.,* 2014, **354**, 163-172.

20 R. P. Tan, J. Carrey and M. Respaud, *Phys. Rev. B*, 2014, **90**, 214421 (12pp).

21 M. Kallumadil, M.Tada, T.Nakagawa, M. Abe, P. Southern, Q. A. Pankhurst, *J. Magn. Magn. Mater.,* 2009, **321,** 1509–1513.

22 S. Laurent, S. Dutz, Urs O Hafeli and M. Mahmoudi, *Advances in Colloid and Interface Science,* 2011, **166,** 8–23.

23 M. Mahmoudi, H. Hofmann, B. Rothen-Rutishauser, and A. Petri-Fink, *Chem. Rev.,* 2012, **112**, 2323-2338.

24 J. Fortin, C. Wilhelm, J. Servais, C. Ménager, J. Bacri, and F. Gazeau, *J. Am. Chem. Soc,.* 2007, **129**, 2628-2635.

25 R. Chen, M. G. Christiansen, and P. Anikeeva, *ACS Nano,* 2013, **7**, 8990-9000.

26 R. Hergt, R. Hiergeist, M. Zeisberger, D. Schüler, U. Heyen, I. Hilger and W. A. Kaiser, *J. Magn. Magn. Mater.*, 2005, **293**, 80-86.

27 C. Binns, P. Prieto, S. Baker, P. Howes, R. Dondi, G. Burley, L. Lari, R. Kröger, A. Pratt, S. Aktas, J. K. Mellon, *J. Nanopart. Res. ,* 2012, **14**,1136 (16pp).

28 E. Pollert, P. Veverka, M. Veverka, O. Kaman, K. Závĕta ,S. Vasseur, R. Epherre, G. Goglio and E. Duguet, *Progress in Solid State Chemistry*, 2009, **37**, 1-14.

29 I. Sharifi, H.Shokrollahi and S.Amiri, *J. Magn. Magn.Mater.*, 2012, **324**, 903–915.

30 M. Menelaou, K. Georgoula, K. Simeonidis and C. Dendrinou-Samara, *Dalton Trans.*, 2014, **43**, 3626

31 D. S. Nikam, S.V. Jadhav, V.M. Khot, M.R. Phadatare, S.H. Pawar, *J. Magn.Magn.Mat.*, 2014, **349,** 208–213.

32 A. Doaga, A.M. Cojocariu, W. Amin, F. Heib, P. Bender, R. Hempelmann, O.F. Caltun, *Materials Chemistry and Physics*, 2013, **143,** 305-310

33 G. Vallejo-Fernandez, O. Whear, A. G. Roca, S. Hussain, J. Timmis, V. Patel and K. O'Grady, *J. Phys. D: Appl. Phys.,* 2013, **46,** 31200 1(6pp).

34 Q. A. Pankhurst, N. T. K. Thanh, S. K. Jones and J. Dobson, *J. Phys. D: Appl. Phys.,* 2009, **42**, 224001 (15pp).

35 R. E. Rosensweig, *J. Magn. Magn. Mater.*, 2002, **252**, 370-374.

36 I. Anreu and E. Natividad, *Int. J. Hyperthermia,* 2013, **29,** 739-751.

37 R. Hergt, S. Dutz and M. Zeisberger, *Nanotechnology,* 2010, **21**, 015706 (5pp).

38 Q.Zeng, I. Baker, J. A. Loudis, Y. Liao, P. J. Hoopes and J. B. Weaver, *Appl. Phys. Lett.,* 2007, **90**, 233112 (3pp).

39 A. López-Ortega, M. Estrader, G. Salazar-Alvarez, A. G. Roca, J. Nogués, *Physics Reports* in press.

40 A. Masoudi, H. R. M. Hosseini, S. M. S. Reyhani, M. A. Shokrgozar, M. A. Oghabian and R. Ahmadi, *International Journal of Pharmaceutics,* 2012, **439**, 28-40.

41 Z. Zhou, Y. Sun, J. Shen, J. Wei, C. Yu, B. Kong, W. Liu, H. Yang, S. Yang and W. Wang, *Biomaterials*, 2014, **35**, 7470-7478.

42 G. Zhang, Y. Liao and I. Baker, *Materials Science & Engineering C-materials for Biological Applications,* 2010, **30**, 92-97.

43 J. H. Lee, J. Jang, J. Choi, S. Ho Moon, S.Noh, J. Kim, J. G. Kim, Il Sun Kim, K. In Park and J. Cheon, *Nature Nanotechnology,* 2011, **6**, 418–422.

44 S. Noh, W. Na,J. Jang, J.H. Lee, E. J. Lee, S. Ho Moon, Y. Lim, J. Soo Shin, and J. Cheon, *Nano Lett.,*2012, **12**, 3716-3721.

45 P. Guardia, A. Riedinger, S. Nitti, G. Pugliese, S. Marras, A. Genovese, M. E. Materia, C. Lefevre, L. Manna and T. Pellegrino, *J. Mater. Chem. B*, 2014,**2**, 4426-4434.

Nanoscale Accepted Manuscript

46   M. Song, Yu Zhang, S. Hu, L. Song, J. Dong, Z. Chen, N. Gu, *Colloids and Surfaces A: Physicochem. Eng. Aspects*,   2012, **408**, 114– 121.

47   H. Joshi, Yen Po Lin, M. Aslam, P. V. Prasad, E. A. Scultz-Sikma, R. Edelman, T. Meade and V. P. Dravid, *J. Phys. Chem. C,* 2009, **113,** 17761-17767

48   J. Carrey, B. Mehdaoui and M. Respaud,   *J. Appl. Phys.,* 2011, **109**, 083921 (17pp).

49   M. Vasilakaki and K. N. Trohidou, *Phys. Rev. B,* 2009, **79**, 144402 (8pp).

50   K. N. Trohidou, C. M. Soukoulis, A. Kostikas and G. Hadjipanayis, *J. Magn. Magn. Mater.*, 1992, **104-107**, 1587-1588.

51   E. Lima Jr, A. L. Brandl, A. D. Arelaro and G. F. Goya, *J. Appl. Phys.*, 2006, **99**, 083908 (10pp).

52   C. Binns, in *Nanomagnetism: Fundamentals and Applications,* ed. C. Binns and R. E. Palmer, Elsevier, Amsterdam, 2014, vol. 6, ch.6, pp. 217-254.

53   L. Del Bianco, D. Fiorani, A. M. Testa, E. Bonetti, L. Savini and S. Signoretti, *Phys. Rev. B,* 2002,**66**, 174418.

54   B. Mehdaoui, A. Meffr, L.-M. Lacroix, J. Carrey, S. Lachaize, M. Respaud, M. Gougeon and B. Chaudret, *J. Appl. Phys.*, 2010, **107**, 09A324.

55   A. K. Gupta and M. Gupta, *Biomaterials*, 2005, **26,** 3995–4021.

56   K. N. Trohidou, X. Zianni and J. A. Blackman, *IEEE Trans. Magn.*, 1998, **34** (4) 1120-1122.

57   M. Vasilakaki and K. N. Trohidou, *J.Phys.D: Appl.Phys.,* 2008, **41,** 134006 (5pp).

58   K. N. Trohidou, X. Zianni and J. A. Blackman, *J. Appl. Phys.*, 1998, **84**, 2795-2800.

59   G. Salazar-Alvarez, J. Qin, V. Sepelak, I. Bergmann, M. Vasilakaki, K.N.Trohidou, J. D. Ardisson, W. A. A. Mecedo, M. Mikhaylova, M. Muhammed, M. D. Baro and J. Nogues, *J.Am.Chem.Soc.*, 2008, **130** (40) 13234-13239.

60   G. Salas, C. Casado, F. J. Teran, R. Miranda, C. J. Serna and M. Puerto Morales, *J. Mater. Chem.*, 2012, **22**, 21065.